Postprint of: Nosko O., Olofsson U., Effective density of airborne wear particles from car brake materials, Journal of Aerosol Science, Vol. 107 (2017), pp. 94-106, DOI: 10.1016/j.jaerosci.2017.02.014

Effective density of airborne wear particles from car brake materials

Oleksii Nosko*[a], Ulf Olofsson[a]

[a] Department of Machine Design, KTH Royal Institute of Technology,
Brinellvägen 83, Stockholm, 100 44, Sweden

People living in urban environments are subject to high health risks due to various anthropogenic sources of airborne particulate matter, including wear of transport vehicle brakes. Studies of airborne particles often require an estimate of the effective particle density, a property that allows correct matching of mass and size characteristics measured by different aerosol instruments. In this study we investigated the effective density of airborne wear particles emitted from car brake materials. The particles were generated by a pin-on-disc machine located in a sealed chamber. Two methods were used to determine the effective density. The first method is based on measurements of PM10 and particle size distribution. The second method involves measurements and subsequent fitting of the mobility size distribution and aerodynamic size distribution. Results from the two methods showed good agreement. It was found that the effective density is 0.75 ± 0.2 g/cm^3. The particle emission, size distribution and effective density are sensitive to temperature variations. An intensive emission of ultrafine particles is initiated at the disc temperature of 185 ± 16 °C. The effective density decreases with the temperature in the interval 110 to 360 °C. There is a large difference between the effective density and the density of the particle material, which suggests that the particles are porous.

Keywords: pin-on-disc; brake wear; airborne particles; aerosol measurement; effective particle density.

Given name	Family name
Oleksii	Nosko
Ulf	Olofsson

* Corresponding author. E-mail: nosko@kth.se (O. Nosko).

Notation

d	particle diameter, μm
d_{a}	aerodynamic diameter, μm
d_{b}	mobility diameter, μm
d_i	midpoint of the i-th stage, μm
i, j	index variables
$k_i(\cdot)$	kernel function of the i-th ELPI+ stage
m	particle mass concentration, μg/m^3
m_{p}	particle mass, g
n	number of the ELPI+ stages, n = 14
p	contact pressure, MPa
v	sliding velocity, m/s
v_{s}	steady sliding velocity, m/s
C	particle concentration, no/cm^3
$C_{\mathrm{c}}(\cdot)$	slip correction factor
$D(\cdot)$	particle mobility size distribution, no/(μm cm^3)
$E_i(\cdot)$	collection efficiency function of the i-th ELPI+ stage
$E_{\mathrm{ch}}(\cdot)$	ELPI+ charger efficiency function, fA cm^3
I_i	electrical current at the i-th ELPI+ stage, fA
I_{si}	simulated electrical current at the i-th stage, fA
N_i	particle concentration at the i-th stage, no/cm^3
T	disc temperature, °C
T_{s}	stationary disc temperature, °C
T_{u}	critical temperature, °C
V_{a}	apparent particle volume, cm^3
V_i	volume of the i-th phase of the particle, cm^3
V_{p}	volume of the material in the particle, cm^3
V_{v}	volume of the void space in the particle, cm^3
ε	deviation of I_{si} from I_i
ρ	variable parameter (effective particle density), g/cm^3
ρ_0	unit density, ρ_0 = 1 g/cm^3
ρ_{e1}, ρ_{e2}	effective particle density (first and second definitions), g/cm^3
ρ_i	density of the i-th phase of the particle, g/cm^3

ρ_m	particle material density, g/cm^3
ρ_p	particle density, g/cm^3
ϕ	particle porosity
APM	Aerosol particle mass analyser
APS	Aerodynamic particle sizer
DMA	Differential mobility analyser
ELPI	Electrical low pressure impactor
FMPS	Fast mobility particle sizer
LM	Low-metallic material
MOUDI	Micro-orifice uniform deposit impactor
NAO	Non-asbestos organic material
OPS	Optical particle sizer
PM10	Mass concentration of particles smaller than 10 μm, μg/m^3
SM	Semi-metallic material
SMPS	Scanning mobility particle sizer
TEOM	Tapered element oscillating microbalance

1. Introduction

Airborne particulate matter can be detrimental to human health. Particles penetrate the human body continuously through breathing, drinking, eating, and skin contact. Inhaled submicron particles reach the deepest parts of the lungs and enter the bloodstream (Oberdörster et al., 2005). Correlations were found between high concentrations of airborne particulate matter and increased morbidity due to various diseases (Gasser et al., 2009; Pope III et al., 2002). People living in urban environments are subject to higher health risks due to airborne particles from various anthropogenic sources (Vu et al., 2015), including the burning of fossil fuels to generate electricity, construction, demolition, and transport vehicles. The latter has an especially significant influence in the vicinity of traffic arteries (Furusjö et al., 2007; Pant and Harrison, 2013). The main sources of traffic-related particles are combustion of fuel in the engine, vehicle-caused turbulence, wear of the road surfaces, and wear of vehicle friction components (Amato et al., 2014; Gietl et al., 2010). Modern cars are equipped with disc brakes in which braking torque is provided by the friction of two pads against a disc. The disc is usually cast iron. Most of the pad materials fall into three classes: low-metallic (LM), non-asbestos organic (NAO), and semi-metallic (SM). During braking, wear particles are emitted from the friction surfaces of the pads and disc, and some of these particles become airborne and are released to the environment. Car brakes contribute considerably to traffic-related particulate matter (Hjortenkrans et al., 2007; Thorpe and Harrison, 2008).

A number of studies have investigated car brake materials in relation to airborne wear particle emissions and associated ecological problems (Grigoratos and Martini, 2015). Garg et al. (2000) studied particle emissions from brakes with NAO and SM pads using a brake dynamometer. The particle emission rate and aerodynamic size distribution were obtained using a Dekati electrical low pressure impactor (ELPI) with 0.03–10 μm aerodynamic diameter range, an MSP micro-orifice uniform deposit impactor (MOUDI) with 0.1–18 μm aerodynamic diameter range, and a TSI electrical aerosol analyser which counts particles larger than 0.01 μm in aerodynamic diameter. Sanders et al. (2003) investigated wear debris from brakes with LM, NAO and SM pads. The tests were conducted on a brake dynamometer in two regimes: wind tunnel and test track. The measurements were made using an ELPI, a MOUDI, and a TSI aerodynamic particle sizer (APS) with 0.5–20 μm aerodynamic diameter range. Iijima et al. (2007) investigated abrasion dusts from a brake dynamometer with NAO pads. A Tokyo Dylec APS was used to classify particles in the aerodynamic diameter range of 0.5 to 20 μm.

Kukutschová et al. (2011) performed a brake dynamometer study of particles emitted from brakes with LM pads. The measurements were made using a 0.01–0.445 μm range TSI scanning mobility particle sizer (SMPS) and a TSI APS. Wahlström at al. (2010a, 2010b, 2012) conducted laboratory and field studies of particulate matter emissions from LM and NAO brake materials. The

particles were counted and classified by size using a 0.02–1 μm range TSI P-Trak condensation nuclei counter, a 0.02–0.3 μm range NanoCheck sensor, a 0.25–32 μm range GRIMM optical aerosol spectrometer, and a 0.1–10 μm range TSI DustTrak aerosol monitor (DustTrak). Hagino et al. (2015) investigated particle emissions from a brake dynamometer with NAO pads under different driving conditions. The particle mass concentrations were measured by two DustTrak II particle mass monitors. Alemani et al. (2015) performed a pin-on-disc study of particles generated by LM / cast iron and NAO / cast iron pairs under steady sliding conditions. The measurements were made using a Dekati ELPI+ with 0.006–10 μm aerodynamic diameter range, a 0.0056–0.56 μm range TSI fast mobility particle sizer (FMPS), and a 0.3–10 μm range TSI optical particle sizer (OPS). Nosko et al. (2015) investigated the influence of temperature on particle emissions from LM / cast iron pairs using a pin-on-disc machine in a sealed chamber. The particles were counted and size classified by an FMPS and an OPS.

This literature review shows that airborne particles generated by car brakes have been investigated in terms of concentration and size distribution. Nonetheless, the quantification of wear particles remains a difficult task because of the differing size and mass characteristics measured by different aerosol instruments. For example, particle emissions can be described in terms of a mobility size distribution and an aerodynamic size distribution (Charvet et al., 2015; Maricq et al., 2000), a measured particle mass concentration and a mass concentration calculated from a particle size distribution (Kousaka et al., 1981; Pitz et al., 2003), an aerodynamic diameter of a particle and its geometric diameter (Kasper, 1977), or a mobility diameter of a particle and its mass (McMurry et al., 2002). In most cases, the mentioned difficulty can be overcome if the so-called effective particle density is known. The effective density is an aerosol property that is intimately connected to the particles' dynamic, optical and chemical properties. It serves as a link between important characteristics of an aerosol particle (DeCarlo et al., 2004), for example, between its mass and apparent volume, between its mobility diameter and aerodynamic diameter, or between its density and dynamic shape factor. The effective density is critical for accurate prediction of particle behaviour in the atmosphere and the human respiratory system in order to efficiently calibrate and utilise air cleaning devices and aerosol measurement instruments.

Literature analysis shows that the effective density has been comprehensively investigated for certain aerosols, including urban and non-urban atmospheres (Hänel and Thudium, 1977; Karg, 2000; Khlystov et al., 2004; Stein et al., 1994), cigarette smoke (Kousaka et al., 1981; Lipowicz, 1988), diesel exhaust (Ahlvik et al., 1998; Kerminen et al., 1999; Keskinen et al., 1998; Slowik et al., 2004), metals (Hering and Stolzenburg, 1995; Ristimäki et al., 2002; Schleicher et al., 1995), and sodium chloride (Kasper, 1977; Kelly and McMurry, 1992; Zelenyuk et al., 2006). To the best of our knowledge, there are no similar published investigations for brake wear particles. When the

effective density of these particles is required, it is usually set equal to some value based on rough estimates and intuitive reasoning. For example, it was assumed to be 1 g/cm^3 (Garg et al., 2000), 5 g/cm^3 (Sanders et al., 2003), or 2.65 g/cm^3 (Wahlström et al., 2010a). The aim of this study was to systematically investigate the effective density of airborne wear particles emitted from car brake materials.

2. Effective particle density definitions and determination methods

Particle material density ρ_{m} (or true particle density) is the average density of the material in the particle:

$$\rho_{\mathrm{m}} = \frac{m_{\mathrm{p}}}{V_{\mathrm{p}}} = \frac{\sum \rho_i V_i}{\sum V_i} \tag{1}$$

where m_{p} is the particle mass; V_{p} is the volume of the material in the particle; V_i and ρ_i are the volume and density of the i-th phase of the particle, respectively.

Particle density ρ_{p} takes internal voids of the particle into account and is defined as

$$\rho_{\mathrm{p}} = \frac{m_{\mathrm{p}}}{V_{\mathrm{p}} + V_{\mathrm{v}}} = \frac{\sum \rho_i V_i}{\sum V_i + V_{\mathrm{v}}} \tag{2}$$

where V_{v} is the volume of the void space in the particle. If we define the particle porosity as the volume fraction ϕ of the internal voids of the particle, that is,

$$\phi = \frac{V_{\mathrm{v}}}{V_{\mathrm{p}} + V_{\mathrm{v}}}$$

then Eqs.(1) and (2) yield the following relationship between ρ_{p} and ρ_{m}:

$$\rho_{\mathrm{p}} = (1 - \phi)\rho_{\mathrm{m}}$$

Effective particle density can be defined in different ways (DeCarlo et al., 2004; Schmid et al., 2007). A common (first) definition of the effective density, ρ_{e1}, is the ratio of the particle mass m_{p} to the apparent particle volume V_{a}:

$$\rho_{\mathrm{e1}} = \frac{m_{\mathrm{p}}}{V_{\mathrm{a}}} \tag{3}$$

The effective density of Eq.(3) was determined for various aerosols using an aerosol particle mass analyser (APM) and a differential mobility analyser (DMA) (Geller et al., 2006; Lee et al., 2009; Malloy et al., 2009; McMurry et al., 2002; Park et al., 2003; Rissler et al., 2014).

When performing measurements for a population of particles, the particle mass concentration m and size distribution (d_i, N_i) can be obtained. Assuming a spherical shape for particles, Eq.(3) is transformed into

$$\rho_{\mathrm{e1}} = \frac{m}{\frac{\pi}{6}\sum N_i d_i^3} \tag{4}$$

where d_i is the midpoint of the i-th stage and N_i is the particle concentration at the i-th stage. A Thermo Fisher Scientific tapered element oscillating microbalance (TEOM) has often been employed to determine m in the form of PM10 (mass concentration of particles smaller than 10 μm) or PM2.5 (mass concentration of particles smaller than 2.5 μm). The effective density of Eq.(4) was determined for atmospheric aerosols in a TEOM–DMA – laser aerosol spectrometer study by Pitz et al. (2003) and a TEOM–SMPS–APS study by Khlystov et al. (2004).

An alternative (second) definition of the effective density, $\rho_{\mathrm{e}2}$, is based on the relationship between the mobility diameter d_{b} and aerodynamic diameter d_{a}:

$$\rho_{\mathrm{e}2} d_{\mathrm{b}}^2 \, C_{\mathrm{c}}(d_{\mathrm{b}}) = \rho_0 d_{\mathrm{a}}^2 \, C_{\mathrm{c}}(d_{\mathrm{a}}) \qquad (5)$$

where ρ_0 is the unit density, ρ_0 = 1 g/cm^3; $C_{\mathrm{c}}(\cdot)$ is the slip correction factor. There are several methods of determining $\rho_{\mathrm{e}2}$ based on Eq.(5). One of them first classifies the particles according to the mobility diameter d_{b} and then measures the aerodynamic diameter d_{a}. This method was implemented using a DMA–MOUDI (Kelly and McMurry, 1992; Stein et al., 1994). Other studies used a DMA – hypersonic impactor (Hering and Stolzenburg, 1995) or a mobility analyser – ELPI (Rostedt et al., 2009). The diameters d_{b} and d_{a} can also be measured in parallel, as was done in SMPS – aerosol mass spectrometer studies by Katrib et al. (2005) and Dinar et al. (2006).

Another method to determine $\rho_{\mathrm{e}2}$ uses parallel measurements of the mobility size distribution and aerodynamic size distribution, followed by fitting these two distributions (Karg, 2000; Kerminen et al., 1999; Maricq et al., 2000; Virtanen et al., 2004). We shall consider this method as an example of using an ELPI+ in tandem with an FMPS. The ELPI+ measures the aerodynamic size distribution. The particles under study are first charged in a corona charger. The charge that is transmitted to another particle depends on d_{b}. The charged particles are then separated according to d_{a} into n = 14 stages. The electrical current I_i produced by the charged particles at each i-th stage is measured by an electrometer. Simultaneously, the FMPS measures the mobility size distribution $D(d_{\mathrm{b}})$. By multiplying $D(d_{\mathrm{b}})$ by the ELPI+ charger efficiency function $E_{\mathrm{ch}}(d_{\mathrm{b}})$ and passing the resulting product through a so-called kernel function $k_i(d_{\mathrm{b}}, \rho)$, one can simulate the electrical current at the i-th stage (Ristimäki et al., 2002):

$$I_{si} = \int_0^\infty k_i(d_{\mathrm{b}}, \rho) \, E_{\mathrm{ch}}(d_{\mathrm{b}}) \, D(d_{\mathrm{b}}) \mathbb{d} d_{\mathrm{b}} \,, \qquad i = 1,2, \dots, n$$

where ρ is the variable parameter (effective density). The kernel functions $k_i(d_{\mathrm{b}}, \rho)$ are determined from the collection efficiency functions $E_i(d_{\mathrm{b}}, \rho)$, $i = 1,2, \dots, n+1$, in the formula below (Järvinen et al., 2014; Marjamäki et al., 2005):

$$k_i(d_{\mathrm{b}}, \rho) = E_i(d_{\mathrm{b}}, \rho) \prod_{j=i+1}^{n+1} \Big(1 - E_j(d_{\mathrm{b}}, \rho)\Big), \qquad i = 1,2, \dots, n$$

The value of ρ that produces a minimum of the deviation ε of I_{si} from I_i is accepted as the effective density, that is,

$$\rho_{e2} = \rho|_{\varepsilon \to \min} \tag{6}$$

The deviation ε can be defined in various ways. One that is commonly used is the least-squares approach:

$$\varepsilon = \sum_{i=1}^{n} \left(\frac{I_{si}}{\sum_{j=1}^{n} I_{sj}} - \frac{I_i}{\sum_{j=1}^{n} I_j} \right)^2 \tag{7}$$

Note that the values of I_{si} need to be normalized before substitution in Eq.(7), so that the particle concentrations associated with I_i and I_{si} are equal to each other.

3. Experimental

The tests were performed using the pin-on-disc machine depicted in Fig.1. The pin sample was a cylinder with a diameter of 10 mm. The height of its wearable part was 10 mm. A dead weight pressed it against a horizontally positioned disc, providing a contact pressure p. The disc had an outer diameter of 63 mm and a thickness of 6 mm. The average friction radius was 25 mm. The disc was driven by a motor with a programmable speed. The temperature T of the disc was measured by a chromel–alumel thermocouple with sliding electrical contact. The hot junction of the thermocouple, 0.5 mm in diameter, was installed at the average friction radius at a distance of 3 mm from the friction surface.

The relative humidity in the test room was 20–30 %, while the temperature was 23–25 °C. The pin-on-disc machine was located inside a sealed chamber. The room air was drawn in by a fan and entered the chamber via a HEPA filter and an inlet. The chamber thus excluded external sources of particles. The particles generated by the friction of the pin sample on the disc were carried by the air to the chamber outlet. The air flow was 2.2 L/s, providing an air exchange rate of 1.3/min.

The air coming out of the chamber was analysed by four aerosol measurement instruments: FMPS 3091, OPS 3330, ELPI+ 2E10-10, and TEOM 1400a. The FMPS classifies 0.0056–0.56 μm particles into 32 stages. The OPS classifies 0.3–10 μm particles into 16 stages. The ELPI+ separates 0.006–10 μm aerodynamic diameter particles into 14 stages. The TEOM measures PM10. The readings from the FMPS, OPS and ELPI+ were sampled at 1 Hz. The PM10 signal was a moving average with a period of 5 min. The instruments were carefully calibrated. Before each test, the chamber and pin-on-disc machine were cleaned, and the whole set-up was checked in the absence of friction. If all the instruments showed zero concentrations, the test was started. Otherwise, the reason for nonzero concentrations was identified and eliminated. This process could include

cleaning the chamber again, checking the impermeability of the inlet tube, or cleaning the ELPI+ impactor components.

Friction pairs corresponding to those used in passenger car brakes were investigated. The disc was cast iron. Six materials code-named M1, …, M6 were used as pin samples. Of these, five materials (M1, …, M5) were LM with phenolic resin as a binder and different reinforcements and abrasives. M6 was an NAO. The pin samples and discs were milled from real brake pads and discs. Their friction surfaces remained unaltered during the milling. The elemental compositions of the pin sample materials obtained by the X-ray diffraction technique can be found in Alemani et al. (2015).

Each test lasted for 90 minutes and included three phases: 15 minute acceleration, 45 minute steady sliding, and 30 minute deceleration. During the acceleration phase, the sliding velocity v at the average friction radius increased linearly from zero to a value v_s. In the steady sliding phase, v was equal to v_s. During the deceleration phase, v decreased linearly to zero. The contact pressure p was constant for the entire test. For each of the six pin sample materials, five tests were done, differing only as regards the load $p \times v_s$: (1) 0.5 MPa × 1.6 m/s; (2) 0.5 MPa × 2.4 m/s; (3) 1 MPa × 1.6 m/s; (4) 1 MPa × 2.4 m/s; (5) 1.5 MPa × 1.6 m/s.

4. Results

Figure 2 presents a plot of the temperature T and sliding velocity v vs. time for a single test. It shows that the change in T follows that of v. In the steady sliding phase, T stabilises about a stationary value T_s. Fig.3 shows the levels of T_s attained in the tests. As would be expected, T_s increases with $p \times v_s$. Thus T_s is 110 to 155 °C at the lowest load of 0.5 MPa × 1.6 m/s, while it exceeds 270 °C at the highest load of 1 MPa × 2.4 m/s or 1.5 MPa × 1.6 m/s.

Figures 4 shows the average value of the particle concentration C measured by both FMPS and OPS. Fig.5 shows the average value of PM10. The averaging was performed in the interval 30 to 60 min, which lies within the steady sliding phase. The substantial increase in C takes place as the load is incremented from 0.5 MPa × 2.4 m/s to 1 MPa × 1.6 m/s. This increase is temperature related. Fig.6, corresponding to the load of Fig.2, clearly shows that as T exceeds a level T_u, which we call 'critical', C increases dramatically. According to the results obtained, such a relationship between T and C holds for all the pin sample materials with $T_u = 185 \pm 16$ °C.

Figure 7 presents particle size distributions observed in the steady sliding phase at temperatures below T_u. The FMPS distribution has a peak at the 24th stage with the midpoint of 0.165 μm. The ELPI+ distribution exhibits a local peak at the 5th stage with the midpoint of 0.119 μm in the aerodynamic diameter scale. The ELPI+ also indicates particles at the lowest stages 1 to 3. The OPS distribution agrees well with the FMPS distribution in the overlapping diameter range.

At temperatures above T_u, the particle size distributions have a completely different form, as illustrated in Fig.8. The substantial increase in C at $T = T_u$, shown in Fig.6, is due to the generation of ultrafine particles (d < 0.1 μm). The FMPS and ELPI+ show similar distributions in the ultrafine particle zone. The FMPS distribution peaks at 0.011–0.029 μm (stages 5 to 12), while the ELPI+ distribution has a maximum at 0.01 μm (stage 1).

The effective density ρ_{e1} was calculated by Eq.(4) based on the data from the TEOM, OPS, and FMPS. PM10 was used as m. The particle size distribution (d_i, N_i) used in the calculations included 45 stages. The first 32 stages coincided with the FMPS stages that cover the 0.0056–0.56 μm range. Stages 33 to 45 corresponded to the OPS stages 4 to 16, which cover the 0.58–10 μm range. Thus, the particle size distribution covered the diameter range 0.0056 to 10 μm (except for a negligibly short interval 0.56 to 0.58 μm), which corresponds to ultrafine, fine (0.1 μm < d < 2.5 μm) and coarse (d > 2.5 μm) particles. Fig.9 shows the values of ρ_{e1} averaged in the interval 30 to 60 min. It was found that ρ_{e1} is 0.75 ± 0.2 g/cm^3 for almost all the tests, although there were individual cases when ρ_{e1} was as small as 0.46 g/cm^3 or as large as 1.08 g/cm^3.

Of special interest is the effective density of ultrafine particles which predominate over fine and coarse particles at temperatures above T_u (see Fig.8). The effective density ρ_{e2} of the ultrafine particles was determined by the method of Eq.(6), based on the ELPI+ and FMPS distributions. As described in the section 2, this method involves minimisation of the deviation ε of the simulated electrical currents I_{si} from the ELPI+ electrical currents I_i. For example, Fig.10 shows an ELPI+ electrical current distribution I_i and three electrical current distributions I_{si} simulated for different values of the parameter ρ. It is seen that as ρ increases, the peak of I_{si} shifts in the direction of larger particle densities. Fig.11 shows the relationship between ε and ρ, determined by Eq.(7). ε has a minimum at $\rho = \rho_{e2}$ = 0.67 g/cm^3, which corresponds to the best fit between I_{si} and I_i. The calculations for all the pin sample materials were done in this manner. Fig.12 shows the values of ρ_{e2} averaged in the interval 30 to 60 min. ρ_{e2} is 0.76 ± 0.1 g/cm^3.

Figure 13 shows the relationship between the effective density and stationary temperature T_s. The two dashed lines show the trends in the data. It is seen that ρ_{e1} and ρ_{e2} tend to decrease with T_s in the intervals 110–360 °C and 190–360 °C, respectively.

5. Discussion

Figures 4 and 6 suggest that temperature has a strong influence on the airborne wear particle emission. Similar influence was previously observed. Garg et al. (2000) investigated particle emissions from brakes with NAO and SM pads. The brake dynamometer tests showed that the particle number per stop increases by 1 to 2 orders of magnitude as the rotor temperature increases

from 200 to 400 °C. This result was obtained using a 0.03–10 μm aerodynamic diameter range ELPI and a TSI electrical aerosol analyser counting particles larger than 0.01 μm in aerodynamic diameter. However, the particle counts from the electrical aerosol analyser were 6 to 7 orders of magnitude larger than those from the ELPI, from which it was concluded that most of the particles emitted were smaller than 0.03 μm. Wahlström at al. (2012) conducted a pin-on-disc study of LM / cast iron pairs placed in a sealed chamber. A 0.02–1 μm range P-Trak found a 2 to 3 orders of magnitude increase in the particle concentration as the pin temperature rose from approximately 170 to 240 °C. At the same time, changes in the pin temperature had no significant effect on the particle concentrations measured by a 0.25–32 μm range GRIMM optical aerosol spectrometer and a 0.1–10 μm range DustTrak. The results of Garg et al. (2000) and Wahlström at al. (2012) mentioned above agree well with those presented in Fig.8, according to which most of the particles are 0.011 to 0.029 μm in diameter at temperatures above T_{u}. Alemani et al. (2015) investigated the materials M1, …, M6 against cast iron. FMPS measurements showed that the ultrafine particle concentration increases by several orders of magnitude as the temperature exceeds 165–190 °C, which is consistent with the critical temperature range of T_{u} = 185 ± 16 °C obtained in the present study. It is notable that the emission rate of the ultrafine particles decays as T goes below T_{u} in the deceleration phase (see Fig.6).

According to the results presented in Figs.9 and 12, the effective densities ρ_{e1} = 0.75 ± 0.2 g/cm^3 and ρ_{e2} = 0.76 ± 0.1 g/cm^3 obtained by the different methods are in a good agreement. Their average values are very close to each other. The variation range of ρ_{e2} lies within the variation range of ρ_{e1}. Moreover, both ρ_{e1} and ρ_{e2} decrease with the stationary temperature T_{s}, as shown in Fig.13. The particle size distributions presented in Fig.7 are also noteworthy. As mentioned in the section 4, the FMPS distribution peaks at 0.165 μm, while the ELPI+ distribution has a local peak at 0.119 μm in the aerodynamic diameter scale. These two peaks most probably correspond to the same particles. The substitution of d_{b} = 0.165 μm and d_{a} = 0.119 μm into Eq.(5) gives the effective density equal to 0.64 g/cm^3, which is within the variation range of ρ_{e1} = 0.75 ± 0.2 g/cm^3.

To our knowledge no measurements of the effective density of brake wear particles have previously been reported. According to the experimental data (Karg, 2000; Khlystov et al., 2004; McMurry et al., 2002; Pitz et al., 2003; Stein et al., 1994), the effective density of non-urban atmospheric aerosols as well as urban atmospheric aerosols, although measured at a distance from the anthropogenic sources of particles, is 1.1 to 3.6 g/cm^3. However, measurements conducted in the vicinity of traffic arteries revealed a significant amount of particulate matter with lower effective densities. For example, Geller et al. (2006) investigated atmospheric aerosols sampled at various locations of the Los Angeles Basin in the USA. Based on the readings from an SMPS and an APM, the average effective density of 0.05–0.4 μm particles was found to be 0.3–1.2 g/cm^3 for a

heavy-duty diesel vehicle freeway and 0.3–1.6 g/cm^3 for a gasoline vehicle freeway. Rissler et al. (2014) performed a study of atmospheric aerosols in an open street canyon in central Copenhagen, Denmark. By using a DMA–APM system, they detected 0.05–0.4 μm particles with an effective density of 0.3 to 0.9 g/cm^3. Thus, the effective density of 0.75 ± 0.2 g/cm^3 obtained in this study is typical for atmospheric aerosols near traffic arteries.

In the study by Alemani et al. (2015), airborne particles emitted from the materials M1, …, M6 against cast iron were collected on ELPI+ filters and analysed for elemental composition by energy-dispersive X-ray spectroscopy. Calculations using a formula equivalent to Eq.(1) showed that the particle material density ρ_{m} of the 0.06–10 μm aerodynamic diameter particles is 2.6 ± 0.5 g/cm^3. This implies that the effective density obtained in this study is approximately 3.5 times smaller than ρ_{m}. Two factors that affect the difference between the effective density and ρ_{m} are the particle porosity and particle shape. The influence of these factors is discussed next.

Lee et al. (2009) investigated the effective density ρ_{e1} of artificially generated porous particles using a DMA–APM system. The porous particles consisted of 0.005 μm silica particles with ρ_{m} = 2.2 g/cm^3. They represented 0.3 μm spheres, i.e. $\rho_{\mathrm{e1}} \approx \rho_{\mathrm{p}}$, but differed in pore size and hence in the porosity ϕ. The tests clearly demonstrated that ρ_{e1} decreases substantially with ϕ. For instance, the particles with $\phi \approx 0.58$ had $\rho_{\mathrm{m}}/\rho_{\mathrm{e1}} \approx 2.4$, while those with $\phi \approx 0.69$ had $\rho_{\mathrm{m}}/\rho_{\mathrm{e1}} \approx 3.2$. Zelenyuk et al. (2006) investigated the dynamic shape factor and effective density ρ_{e2} of various irregularly shaped particles: 0.1–1 μm particles of polystyrene latex (agglomerated shape), ammonium sulphate (rounded shape), sodium chloride (angular shape). The determination of ρ_{e2} was based on measurements by a DMA and a single particle laser ablation time-of-flight mass spectrometer. The study revealed a noticeable influence of the particle shape irregularity on ρ_{e2}, with the ratio $\rho_{\mathrm{p}}/\rho_{\mathrm{e2}}$ between 1 and 1.9. Thus, according to the experimental data by Lee et al. (2009) and Zelenyuk et al. (2006), the 3.5 time difference between the effective density and ρ_{m} found in this study is most probably caused by both particle porosity and particle shape. Our reasoning leads to the hypothesis that airborne wear particles generated by car brakes are porous. This hypothesis will be verified in our future studies.

6. Conclusions

The effective density of airborne wear particles emitted from car brake materials was investigated using two different methods. The particulate matter mass – particle size distribution method of Eq.(4) is based on measurements of PM10 and particle size distribution. The mobility diameter – aerodynamic diameter method of Eq.(6) involves measurements and subsequent fitting

of the mobility size distribution and aerodynamic size distribution. The study led to the following conclusions:

1. The particulate matter mass – particle size distribution method and mobility diameter – aerodynamic diameter method show good agreement in determining the effective density of airborne wear particles as applied to car brake materials.
2. The effective density is 0.75 ± 0.2 g/cm^3 for the LM and NAO pad materials against cast iron. It is typical for atmospheric aerosols near traffic arteries.
3. The effective density is approximately 3.5 times smaller than the density of the particle material, which is most probably due to the particle porosity and shape.
4. The emission rate of ultrafine particles increases substantially as the temperature exceeds the critical level of 185 ± 16 °C and decays as the temperature goes below this critical level.
5. The effective particle density decreases with the temperature in the interval 110 to 360 °C.

The findings of the study can be useful for simulating the dynamic behaviour of wear particles in the atmosphere and the human respiratory system, as well as for finding quantitative relationships between their physical properties.

Vitae

Oleksii Nosko is a researcher at KTH Royal Institute of Technology. He received the Doctor's degree in Tribology in 2010 and the Ph.D. in Mechanical Engineering in 2013. His main research interests include measurement and simulation of temperatures at sliding contacts, thermo-mechanical friction problems, and airborne particle emissions from sliding contacts.

Ulf Olofsson is a Professor in Tribology at KTH Royal Institute of Technology since 2006. He received the Ph.D. in 1996 on a thesis on wear as failure mechanism in boundary lubricated rolling bearings. His main research interests include interfaces and especially simulation and prediction of friction and wear, mainly applied to problems in mechanical, automotive and railway engineering. New research interests include friction modifiers in rolling sliding contacts and joints, airborne particles from wear processes in disc brakes, tyre to road interaction, and human touch tribology.

Acknowledgement

This work was supported by the European Union Seventh Framework Programme (FP-PEOPLE-2012-IAPP) under the Rebrake Project [grant number 324385].

The authors wish to thank Mr Mattia Alemani and Dr Vlastimil Matějka at Brembo S.p.A.; Dr Ibrahim Metinoz at the University of Trento; Mr Magnus Brydolf and Mr Billy Sjövall at

Stockholm Air and Noise Analysis; Mr Peter Ahlvik at ExIS AB; Mr Peter Carlsson, Mr Yezhe Lyu and Ms Yingying Cha at KTH Royal Institute of Technology for their technical assistance.

References

1. Ahlvik, P., Ntziachristos, L., Keskinen, J., & Virtanen, A. (1998). Real time measurements of diesel particle size distribution with an electrical low pressure impactor. *SAE Technical Paper*, 980410.
2. Alemani, M., Nosko, O., Metinoz, I., & Olofsson, U. (2015). A study on emission of airborne wear particles from car brake friction pairs. *SAE International Journal of Materials and Manufacturing*, 9 (1), 147–157.
3. Amato, F., Cassee, F. R., Denier van der Gon, H. A. C., Gehrig, R., Gustafsson, M., Hafner, W., … Querol, X. (2014). Urban air quality: The challenge of traffic non-exhaust emissions. *Journal of Hazardous Materials*, 275, 31–36.
4. Charvet, A., Bau, S., Bémer, D., & Thomas, D. (2015). On the importance of density in ELPI data post-treatment. *Aerosol Science and Technology*, 49 (12), 1263–1270.
5. DeCarlo, P. F., Slowik, J. G., Worsnop, D. R., Davidovits, P., & Jimenez, J. L. (2004). Particle morphology and density characterization by combined mobility and aerodynamic diameter measurements. Part 1: Theory. *Aerosol Science and Technology*, 38 (12), 1185–1205.
6. Dinar, E., Mentel, T. F., & Rudich, Y. (2006). The density of humic acids and humic like substances (HULIS) from fresh and aged wood burning and pollution aerosol particles. *Atmospheric Chemistry and Physics*, 6 (12), 5213–5224.
7. Furusjö, E., Sternbeck, J., & Cousins, A. P. (2007). PM10 source characterization at urban and highway roadside locations. *Science of the Total Environment*, 387 (1–3), 206–219.
8. Garg, B. D., Cadle, S. H., Mulawa, P. A., & Groblicki, P. J. (2000). Brake wear particulate matter emissions. *Environmental Science and Technology*, 34 (21), 4463–4469.
9. Gasser, M., Riediker, M., Mueller, L., Perrenoud A., Blank F., Gehr, P., & Rothen-Rutishauser, B. (2009). Toxic effects of brake wear particles on epithelial lung cells in vitro. *Particle and Fibre Toxicology*, 6, 30.
10. Geller, M., Biswas, S., & Sioutas, C. (2006). Determination of particle effective density in urban environments with a differential mobility analyzer and aerosol particle mass analyzer. *Aerosol Science and Technology*, 40 (9), 709–723.
11. Gietl, J. K., Lawrence, R., Thorpe, A. J., & Harrison, R. M. (2010). Identification of brake wear particles and derivation of a quantitative tracer for brake dust at a major road. *Atmospheric Environment*, 44 (2), 141–146.

12. Grigoratos, T., & Martini, G. (2015). Brake wear particle emissions: A review. *Environmental Science and Pollution Research*, 22 (4), 2491–2504.
13. Hagino, H., Oyama, M., & Sasaki, S. (2015). Airborne brake wear particle emission due to braking and accelerating. *Wear*, 334–335, 44–48.
14. Hänel, G., & Thudium, J. (1977). Mean bulk densities of samples of dry atmospheric aerosol particles: A summary of measured data. *Pure and Applied Geophysics*, 115 (4), 799–803.
15. Hering, S. V., & Stolzenburg, M. R. (1995). On-line determination of particle size and density in the nanometer size range. *Aerosol Science and Technology*, 23 (2), 155–173.
16. Hjortenkrans, D. S. T., Bergbäck, B. G., & Häggerud, A. V. (2007). Metal emissions from brake linings and tires: case studies of Stockholm, Sweden 1995/1998 and 2005. *Environmental Science and Technology*, 41 (15), 5224–5230.
17. Iijima, A., Sato, K., Yano, K., Tago, H., Kato, M., Kimura, H., & Furuta, N. (2007). Particle size and composition distribution analysis of automotive brake abrasion dusts for the evaluation of antimony sources of airborne particulate matter. *Atmospheric Environment*, 41 (23), 4908–4919.
18. Järvinen, A., Aitomaa, M., Rostedt, A., Keskinen, J., & Yli-Ojanperä, J. (2014). Calibration of the new electrical low pressure impactor (ELPI+). *Journal of Aerosol Science*, 69, 150–159.
19. Karg, E. W. (2000). The density of ambient particles from combined DMA and APS data. *Journal of Aerosol Science*, 31 (1), 759–760.
20. Kasper, G. (1977). On the density of sodium chloride aerosols formed by condensation. *Journal of Colloid and Interface Science*, 62 (2), 359–360.
21. Katrib, Y., Martin, S. T., Rudich, Y., Davidovits, P., Jayne, J. T., & Worsnop, D. R. (2005). Density changes of aerosol particles as a result of chemical reaction. *Atmospheric Chemistry and Physics*, 5, 275–291.
22. Kelly, W. P., & McMurry, P. H. (1992). Measurement of particle density by inertial classification of differential mobility analyzer-generated monodisperse aerosols. *Aerosol Science and Technology*, 17 (3), 199–212.
23. Kerminen, V.-M., Mäkelä, T., Hillamo, R., & Rantanen, L. (1999). Relation between particle number and mass size distribution in the diesel car exhaust. *Journal of Aerosol Science*, 30 (1), S777–S778.
24. Keskinen, J., Virtanen, A., Ahlvik, P., & Ntziachristos, L. (1998). Estimation of effective density of diesel particles. *Journal of Aerosol Science*, 29 (S1), S1007–S1008.
25. Khlystov, A., Stanier, C., & Pandis, S. N. (2004). An algorithm for combining electrical mobility and aerodynamic size distributions data when measuring ambient aerosol. *Aerosol Science and Technology*, 38 (S1), 229–238.

26. Kousaka, Y., Okuyama, K., Endo, Y., & Tanaka, H. (1981). Comparison among measuring methods of density of spherical aerosol particles. *Journal of Chemical Engineering of Japan*, 14 (3), 214–218.
27. Kukutschová, J., Moravec, P., Tomášek, V., Matějka, V., Smolik, J., Schwarz, J., … Filip, P. (2011). On airborne nano/micro-sized wear particles released from low-metallic automotive brakes. *Environmental Pollution*, 159 (4), 998–1006.
28. Lee, S. Y., Widiyastuti, W., Tajima, N., Iskandar, F., & Okuyama, K. (2009). Measurement of the effective density of both spherical aggregated and ordered porous aerosol particles using mobility- and mass-analyzers. *Aerosol Science and Technology*, 43 (2), 136–144.
29. Lipowicz, P. J. (1988). Determination of cigarette smoke particle density from mass and mobility measurements in a Millican cell. *Journal of Aerosol Science*, 19 (5), 587–589.
30. Malloy, Q. G. J., Nakao, S., Qi, L., Austin, R., Stothers, C., Hagino, H., & Cocker III, D. R. (2009). Real-time aerosol density determination utilizing a modified scanning mobility particle sizer — Aerosol particle mass analyzer system. *Aerosol Science and Technology*, 43 (7), 673–678.
31. Maricq, M. M., Podsiadlik, D. H., & Chase, R. E. (2000). Size distributions of motor vehicle exhaust PM: A comparison between ELPI and SMPS measurements. *Aerosol Science and Technology*, 33 (3), 239–260.
32. Marjamäki, M., Lemmetty, M., & Keskinen, J. (2005). ELPI response and data reduction I: Response functions. *Aerosol Science and Technology*, 39 (7), 575–582.
33. McMurry, P. H., Wang, X., Park, K., & Ehara, K. (2002). The relationship between mass and mobility for atmospheric particles: A new technique for measuring particle density. *Aerosol Science and Technology*, 36 (2), 227–238.
34. Nosko, O., Alemani, M., & Olofsson, U. (2015). Temperature effect on emission of airborne wear particles from car brakes. Proceedings of Europe's Braking Conference and Exhibition 2015, EB2015-TEF-014. http://dx.doi.org/10.13140/RG.2.1.1237.3209
35. Oberdörster, G., Maynard, A., Donaldson, K., Castranova, V., Fitzpatrick, J., Ausman, K., … Yang H. (2005). Principles for characterizing the potential human health effects from exposure to nanomaterials: Elements of a screening strategy. *Particle and Fibre Toxicology*, 2, 8.
36. Pant, P., & Harrison, R. M. (2013). Estimation of the contribution of road traffic emissions to particulate matter concentrations from field measurements: A review. *Atmospheric Environment*, 77, 78–97.
37. Park, K., Cao, F., Kittelson, D. B., & McMurry, P. H. (2003). Relationship between particle mass and mobility for diesel exhaust particles. *Environmental Science and Technology*, 37 (3), 577–583.

38. Pitz, M., Cyrys, J., Karg, E., Wiedensohler, A., Wichmann, H.-E., & Heinrich, J. (2003). Variability of apparent particle density of an urban aerosol. *Environmental Science and Technology*, 37 (19), 4336–4342.
39. Pope III, C. A., Burnett, R. T., Thun, M. J., Calle, E. E., Krewski, D., Ito, K., & Thurston, G. D. (2002). Lung cancer, cardiopulmonary mortality, and long-term exposure to fine particulate air pollution. *The Journal of the American Medical Association*, 287 (9), 1132–1141.
40. Rissler, J., Nordin, E. Z., Eriksson, A. C., Nilsson, P. T., Frosch, M., Sporre, M. K., … Swietlicki, E. (2014). Effective density and mixing state of aerosol particles in a near-traffic urban environment. *Environmental Science and Technology*, 48 (11), 6300–6308.
41. Ristimäki, J., Virtanen, A., Marjamäki, M., Rostedt, A., & Keskinen, J. (2002). On-line measurement of size distribution and effective density of submicron aerosol particles. *Journal of Aerosol Science*, 33 (11), 1541–1557.
42. Rostedt, A., Marjamäki, M., & Keskinen, J. (2009). Modification of the ELPI to measure mean particle effective density in real-time. *Journal of Aerosol Science*, 40 (9), 823–831.
43. Sanders, P. G., Xu, N., Dalka, T. M., & Maricq, M. M. (2003). Airborne brake wear debris: Size distributions, composition, and a comparison of dynamometer and vehicle tests. *Environmental Science and Technology*, 37 (18), 4060–4069.
44. Schleicher, B., Künzel, S., & Burtscher, H. (1995). In situ measurement of size and density of submicron aerosol particles. *Journal of Applied Physics*, 78, 4416–4422.
45. Schmid, O., Karg, E., Hagen, D. E., Whitefield, P. D., & Ferron, G. A. (2007). On the effective density of non-spherical particles as derived from combined measurements of aerodynamic and mobility equivalent size. *Journal of Aerosol Science*, 38 (4), 431–443.
46. Slowik, J. G., Stainken, K., Davidovits, P., Williams, L. R., Jayne, J. T., Kolb, C. E., … Jimenez, J. L. (2004). Particle morphology and density characterization by combined mobility and aerodynamic diameter measurements. Part 2: Application to combustion-generated soot aerosols as a function of fuel equivalence ratio. *Aerosol Science and Technology*, 38 (12), 1206–1222.
47. Stein, S. W., Turpin, B. J., Cai, X., Huang, P.-F., & McMurry P. H. (1994). Measurements of relative humidity-dependent bounce and density for atmospheric particles using the DMA-impactor technique. *Atmospheric Environment*, 28 (10), 1739–1746.
48. Thorpe, A., & Harrison, R. M. (2008). Sources and properties of non-exhaust particulate matter from road traffic: A review. *Science of the Total Environment*, 400 (1–3), 270–282.
49. Virtanen, A., Ristimäki, J., & Keskinen, J. (2004). Method for measuring effective density and fractal dimension of aerosol agglomerates. *Aerosol Science and Technology*, 38 (5), 437–446.

50. Vu, T. V., Delgado-Saborit, J. M., & Harrison, R. M. (2015). Review: Particle number size distributions from seven major sources and implications for source apportionment studies. *Atmospheric Environment*, 122, 114–132.
51. Wahlström, J., Söderberg, A., Olander, L., Olofsson, U., & Jansson, A. (2010a). Airborne wear particles from passenger car disc brakes: A comparison of measurements from field tests, a disc brake assembly test stand, and a pin-on-disc machine. *Proceedings of the Institution of Mechanical Engineers. Part J: Journal of Engineering Tribology*, 224, 179–188.
52. Wahlström, J., Olander, L., & Olofsson U. (2010b). Size, shape, and elemental composition of airborne wear particles from disc brake materials. *Tribology Letters*, 38 (1), 15–24.
53. Wahlström, J., Olander, L., & Olofsson, U. (2012). A pin-on-disc study focusing on how different load levels affect the concentration and size distribution of airborne wear particles from the disc brake materials. *Tribology Letters*, 46 (2), 195–204.
54. Zelenyuk, A., Cai, Y., & Imre, D. (2006). From agglomerates of spheres to irregularly shaped particles: Determination of dynamic shape factors from measurements of mobility and vacuum aerodynamic diameters. *Aerosol Science and Technology*, 40 (3), 197–217.

Figure captions

All figures — colour online only.

Fig.1. Schematic of the experimental set-up

Fig.2. Temperature T and sliding velocity v vs. time (M1, 1 MPa × 1.6 m/s, T_s = 244 °C)

Fig.3. Stationary temperature T_s

Fig.4. Average values of the particle concentration C

Fig.5. Average values of PM10

Fig.6. Particle concentration C vs. temperature T (M1, 1 MPa × 1.6 m/s, T_s = 244 °C)

Fig.7. Particle size distributions at temperatures below T_u (M2, 0.5 MPa × 2.4 m/s, T_s = 142 °C)

Fig.8. Particle size distributions at temperatures above T_u (M2, 1.5 MPa × 1.6 m/s, T_s = 283 °C)

Fig.9. Effective density ρ_{e1} of coarse, fine and ultrafine particles

Fig.10. Measured and simulated electrical current distributions (M1, 1 MPa × 2.4 m/s, T_s = 322 °C)

Fig.11. Deviation ε vs. parameter ρ

Fig.12. Effective density ρ_{e2} of ultrafine particles

Fig.13. Effective density vs. stationary temperature T_s

Fig.1

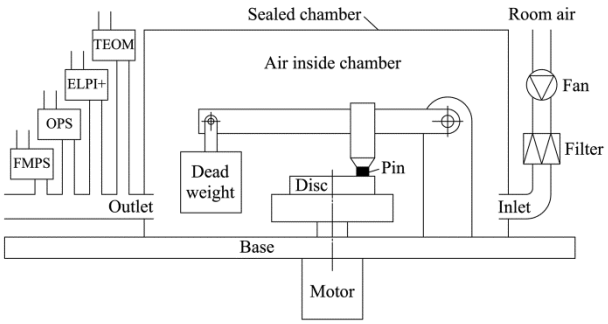

Fig.2

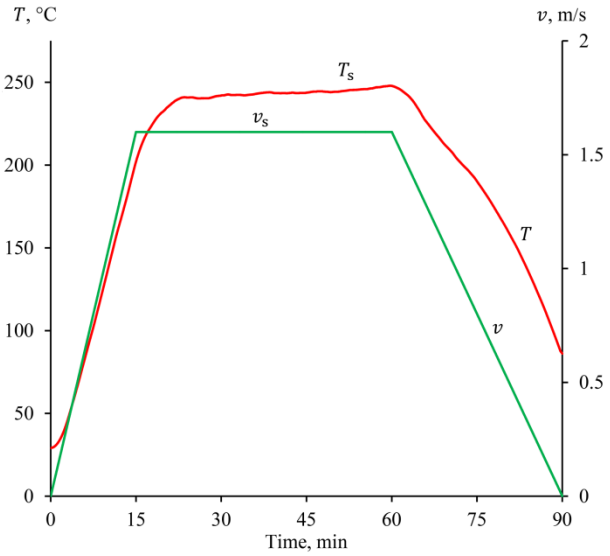

Fig.3

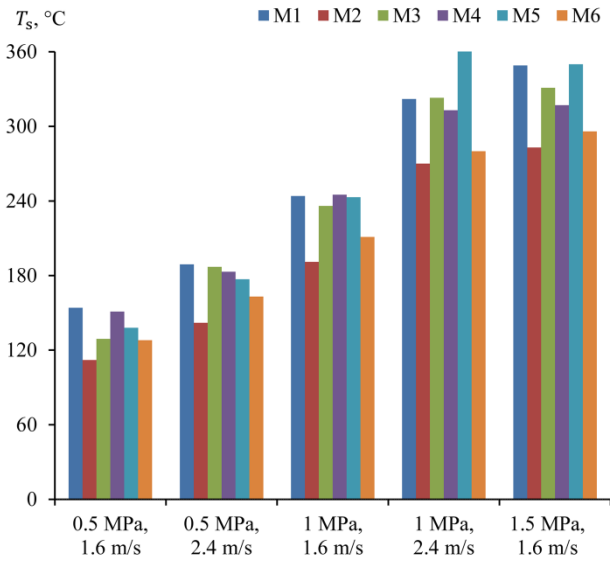

Fig.4

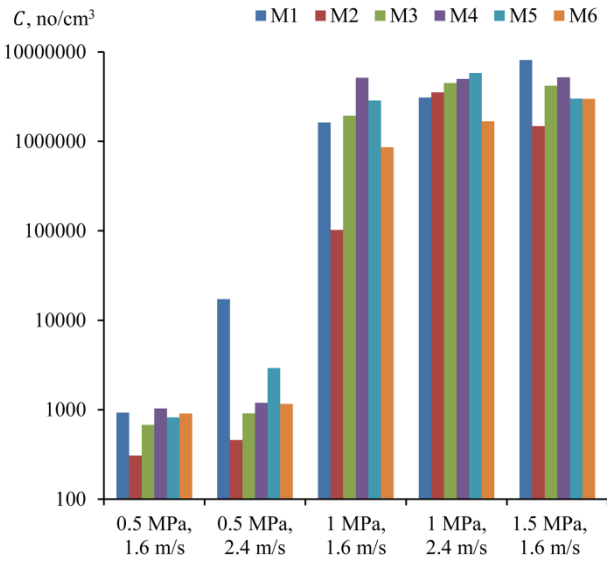

Fig.5

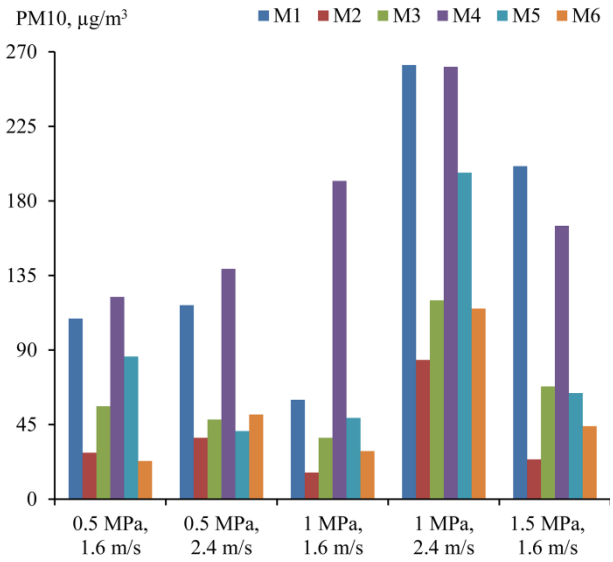

Fig.6

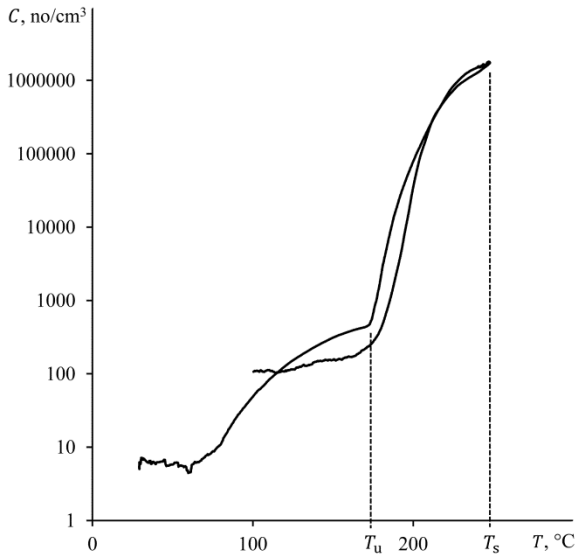

Fig.7

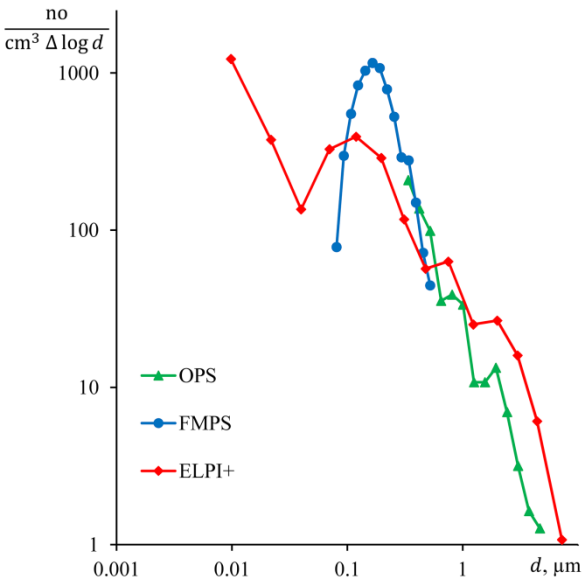

Fig.8

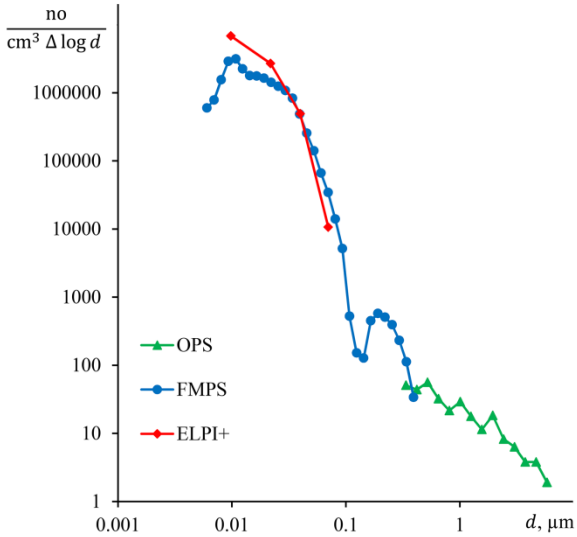

Fig.9

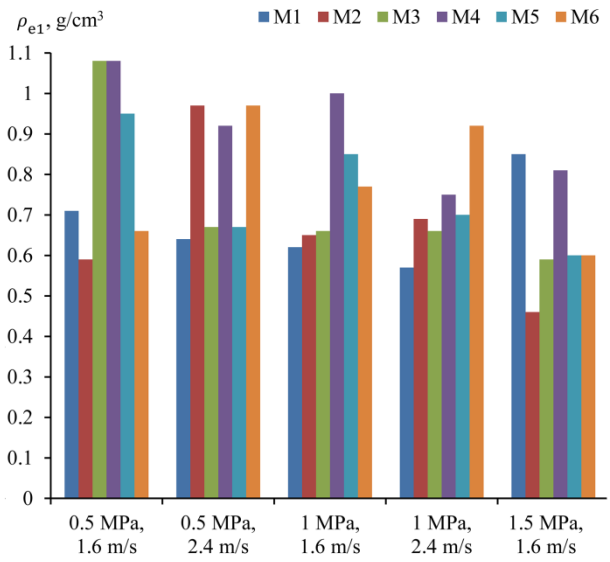

Fig.10

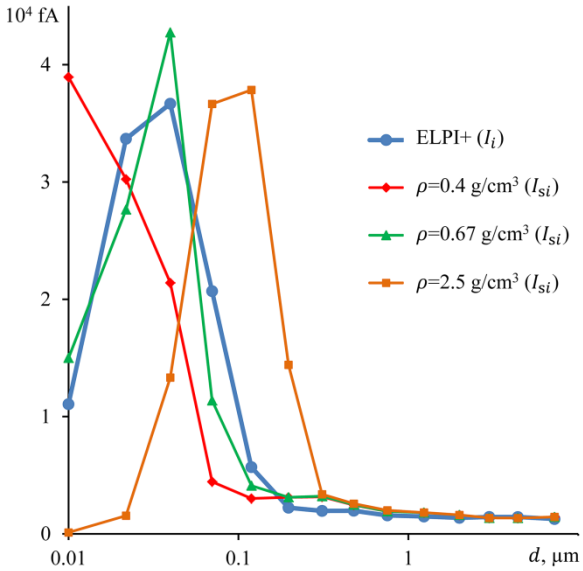

Fig.11

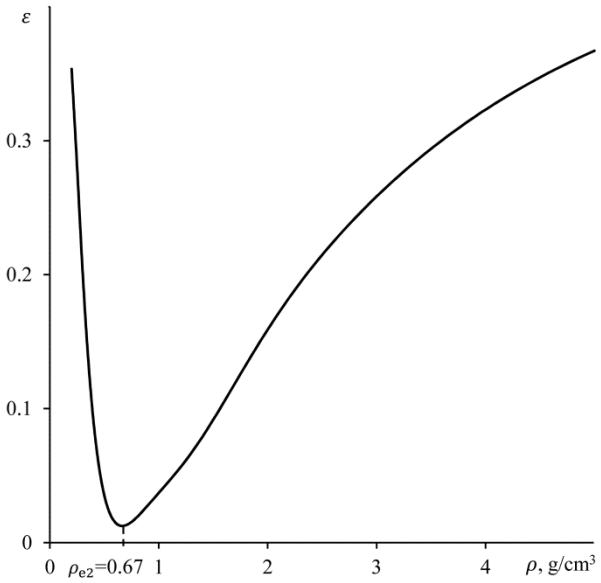

Fig.12

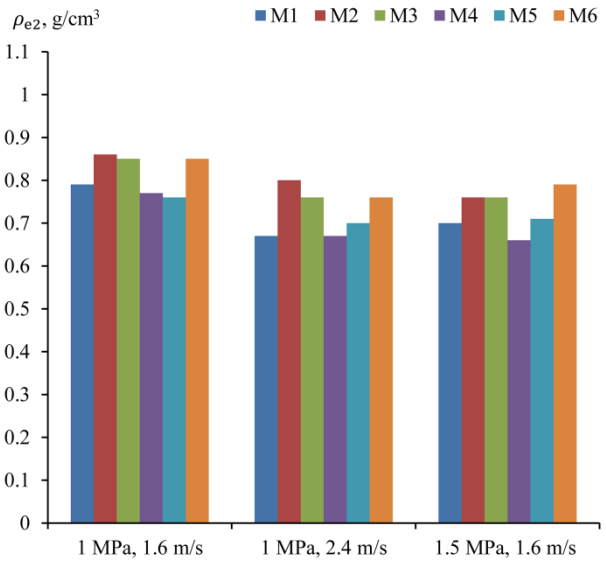

Fig.13

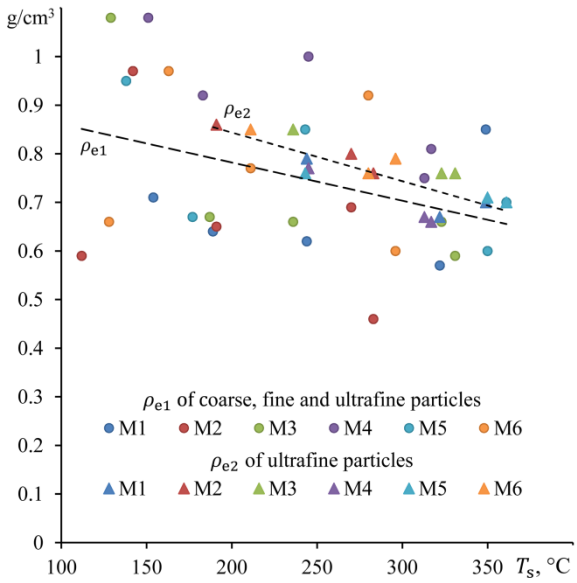

Graph abstract